Total Variation and Tight Frame Iteration Regularization Based Image Reconstruction for Short-scanning Few-view Computer Tomography

Ru Xu[1]
[1]*College of Big Data and Intelligent Engineering, Yangtze Normal University, Chongqing 408100, China*

Keywords: Image Processing, Image reconstruction, Few-view CT, Total variation, Tight frame iteration.

Abstract: The excessive dose of the widely used X-ray computer tomography (CT) may induce potential disease. So lower radiation dose is an important direction of CT development. Short-scanning few-view CT (SSFW-CT) imaging can reduce radiation dose and scan time simultaneously. The total variation (TV) algorithm based on compressed sensing has been extensively used in CT reconstruction. The algorithm based on sparse transform is also applied to CT reconstruction, such as wavelet transform. Because of the serious discomfort with the SSFW-CT, the paper proposes a regularization iteration reconstruction algorithm method that combining total variation method and tight-frame transform, denoted TV-TFIR. The proposed method can reconstruct the details of the image more precisely. The simulation phantom and real data are used to verify the effectiveness of the proposed algorithm. The experimental results of the proposed method are more effective in both quantitative indicators and visual effects.

1 INTRODUCTION

X-ray computed tomography (CT) has been widely used in industrial, clinical diagnosis, and other applications because CT can get the high-resolution internal structure image (Jouini, 2016). However, the extra x-ray radiation exposure during clinical examination may cause cancer and other genetic lesions (Brenner, 2007). So the main research is to reduce the radiation doses and reconstruct the high quality images. There are two main way to reduce the dose: the first way is to reduce the x-ray exposure in each projection views and the second way is to reduce the number of projections. (Wang, G., 2009) The first method will produce noisy projections and the reconstructed image is surrounded by noise and artifacts (Xu, Q., 2012). The second method including sparse-view CT and few-view CT will cause serious artifacts in the reconstructed images for insufficient projection sampling (Yu, W., 2017). Sparse-view CT is usually sampled throughout the circumference. To further reduce the radiation dose, we proposed a reconstruction algorithm combining the total variation and tight frame iteration regularization (TV-TFIR) algorithm for the short-scanning few-view CT.

For the SSFW-CT, the traditional filtering back-projection (FBP) algorithm (Chang, S., 1978) and simultaneous algebraic reconstruction technique (SART) algorithm (Andersen, A. H., 1984) can't reconstruct the high-quality image for incomplete projection data. The development of compressed sensing (CS) theory makes the ill-posed image reconstruction can be effectively solved (Donoho, D. L., 2006). Image reconstruction algorithms based on compressed sensing mainly use prior knowledge of image, especially the sparseness of image such as gradient transform (Laroque, S. J., 2006), wavelet transform (Li, M., 2014) and so on.

Sidky proposed the total variation (TV) algorithm for the limit-angle CT reconstruction (Sidky, E. Y., 2008). And there are many algorithms to solve the TV reconstruction, like fixed point iteration method (Abushammala, M., 2015), primal-dual Newton method (Peng, J., 2000), multilevel optimization methods (Titli, A., 2007). The splitting schemes is an effective method to solve the TV problem, and TV reconstruction method could suppress artifacts and smooth images very well reconstruct high quality images from incomplete

Xu, R.
Total Variation and Tight Frame Iteration Regularization Based Image Reconstruction for Short-scanning Few-view Computer Tomography.
DOI: 10.5220/0008096101030110
In *Proceedings of the International Conference on Advances in Computer Technology, Information Science and Communications (CTISC 2019)*, pages 103-110
ISBN: 978-989-758-357-5

data. (Wang, Y. 2016). Recently, TV algorithm is widely used for different reconstruction tasks (Ritschl, L., 2011). However, Yu and Wang (Yu, H., 2009) indicated that the TV minimization algorithm assumes the image is piecewise constant and that doesn't satisfy the clinical and industrial reality. Furthermore, the result image of TV reconstruction algorithm may suffer from blocky artifacts.

There are other iterative methods can avoid the block artifacts, such as tight frame iteration regularization (TFIR) (Li, M., 2014), nonlocal means (NLM) (Zhang, L., 2018), dictionary learning algorithm (Lu, Y., 2011) and so on. The tight feame iteration reconstruction has been used in short-scanning few-view CT reconstruction because the reconstructed images are sparse under the proper wavelet frame (Gu, J., 2017). The sparsity of wavelet coefficient is restrained by using the quasi-norm.

When the projection data is seriously incomplete, the TV and TFIR methods based on compressed sensing cannot reconstruct high quality images. Li et al. used the TV reconstruction and wavelet tight transform for the limited-angle CT (Li, J., 2018). Inspired by them, we proposed a reconstruction algorithm combining the total variation (TV) and wavelet tight frame regularization for the SSFW-CT reconstruction.

The remain of the paper is organized as follows. Section 2 firstly describes the geometry configuration of the SCFW-CT. Then the TVM algorithm and wavelet tight frame are also introduced in this section. Finally, the total variation combined with tight frame iteration regularization (TV-TFIR) model is proposed and the solution algorithm is given. The experimental results for both digital phantoms and real CT projection data are displayed in Section 3. Section 4 shows the conclusions and the outlook of this paper.

2 SCANNING STRUCTURE AND RECONSTRUCT ALGORITHM

2.1 Scanning Structure Configuration

In this paper, the circular fan-beam short-scanning configuration is adopted. And the sparse-angle sampling is used to further reducing the radiation dose. The scanning geometry is shown in Figure 1. The dashed arc is the rotation orbit. The X-ray source spot S is installed on the rotation orbit, and the detector B was installed on the opposite of the X-ray source. The detector and the X-ray source are relatively fixed and they rotate around the circular orbit during scanning. The object is installed on the center of the rotation system. The detector in the right of Fig. 1 is the double solid arc. For the fan-beam short-scanning problem, the real rotation angle is a part of the circle, and it is represented by θ. The length of OS is the distance between X-ray source to the center of rotation. OB is the distance between the center of rotation to the detector. The whole scanning process is very fast because the sampling angle is sparse.

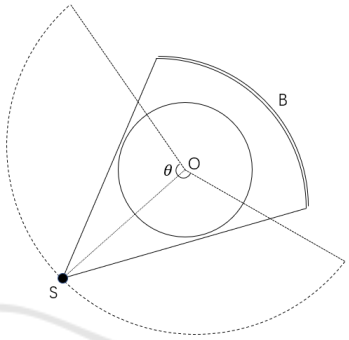

Figure 1: The scanning geometry structure of the short-scanning few-view CT.

2.2 Related Reconstruction Model

The scanning process of SSFW-CT can be discrete and approximated as the following linear system (Hsieh, J., 2000):

$$Af = p + \varepsilon \tag{1}$$

Where $f \in R^N$ is the unknown image. $p \in R^M$ is the projection dat. $A \in R^{M \times N}$ is the system matrix. Where $A_{i,j}$ represents the intersection length of ray-sum to the image pixel, ε is the noise.

In the SSFW-CT, the projection data are severely incomplete. The traditional simultaneous algebraic reconstruction technique (SART) algorithms may lead to serious artifacts. Compressed sensing (CS) is an effective solution to this problem, and CS method requires prior knowledge of the image as the regularization term (Donoho, D. L., 2006). Then, the liner system (1) can be formulated as follows:

$$f^* = \arg\min_f \left\| Af - p \right\|_2^2 + \lambda \cdot R(f) \tag{2}$$

Where $R(f)$ is the regularization term, f^* is the optimal solution to (2). The $\|Af-p\|_2^2$ is the data consistency term.

The SSFW-CT is a serious ill-posed problem. In recent decades, the regularization method has been widely used in CT reconstruction. The regular terms usually use prior knowledge of the image, and the general regular reconstruction algorithm can be expressed as the following minimization optimization problem:

$$\arg\min_{f\in\Omega}\frac{1}{2}\|Af-p\|_2^2+\lambda\|f\|_{\mathrm{TV}} \tag{3}$$

The total variation (TV) norm of the image can be expressed as follow:

$$\|f\|_{TV}=\sum_{i,j}\sqrt{(f_{i,j}-f_{i-1,j})^2+(f_{i,j}-f_{i,j-1})^2} \tag{4}$$

Where $f_{i,j}$ is the gray value of the image f.

The tight frame iteration regularization (TFIR) (Yu, W., 2015) is defined in the follow:

$$\arg\min_{f\in\Omega}\frac{1}{2}\|Af-p\|_2^2+\alpha\|Wf\|_0 \tag{5}$$

Where the $\|Wf\|_0$ is the non-zero number of (Wf).

2.3 Proposed TV-TFIR Model

To reconstruct the better image, we proposed a total variation combined with tight frame iteration reconstruction algorithm for the short-scanning few-view CT.

$$\min_{f\in\Omega}\alpha_1\|z\|_0+\alpha_2\|v\|_1,\ s.t\begin{cases}Af+e=g,\ f\ge 0\\ Df=v\\ Wf=z\end{cases} \tag{6}$$

Where A is the system matrix of the CT. D is total variation operators, and the W is B-spline wavelet transform (Unser, M., 1992). To effectively solve problem (5), we use the alternating minimization method (ADM) algorithm in this paper (Wang, Y. 2016).

The constrained optimization above can be transformed into an unconstrained optimization problems using the augmented Lagrangian method. And then we use the ADM to solve the augmented Lagrangian (AL) function of formula (6). The corresponding AL function is as follows:

$$\begin{aligned}\min_{z,v,f}\mathrm{L}(z,v,f)&=\alpha_1\|z\|_0+\alpha_2\|v\|_1\\&+\gamma_1^T(Wf-z)+\frac{\lambda_1}{2}\|Wf-z\|_2^2+\gamma_2^T(Df-v)\\&+\frac{\lambda_2}{2}\|Df-v\|_2^2+\gamma_3^T(Af-g)+\rho\|Af-g\|_2^2\end{aligned} \tag{7}$$

Where γ_1,γ_2 and γ_3 are the Lagrange multipliers, and the positive constants λ_1,λ_2 and ρ are used to balance the data consistency item. The ADM splits the AL function (7) into three sub-problems, L(f), L(z) and L(v). Then the sub-problems of (7) can be solved as following iterations:

The first sub-problem about f is L(f):

$$\begin{aligned}f^*=\arg\min_f\mathrm{L}(f)&=\gamma_1^T(Wf-z)+\frac{\lambda_1}{2}\|Wf-z\|_2^2\\&+\gamma_2^T(Df-v)+\frac{\lambda_2}{2}\|Df-v\|_2^2\\&+\gamma_3^T(Af-g)+\rho\|Af-g\|_2^2\end{aligned} \tag{8}$$

The formula is a quadratic function about f. So the exact minimizer solution of (8) is:

$$\begin{aligned}f^*=(&\lambda_1 I+\lambda_2 D^TD+2\rho A^TA)^+(\lambda_1W^Tz\\&-W^T\gamma_1+\lambda_2D^Tv-D^T\gamma_2+2\rho A^Tg-A^T\gamma_3)\end{aligned} \tag{9}$$

The W^T is the transpose of the wavelet transform matrix W. Suppose and the matrix X^+ is the pseudo-inverse of X, where X could be any matrix. In this problem, the storage and computational complexity of pseudo-inverse matrix of W is very high for the large scale of matrix A. An efficient solution is to use the proximal point algorithm (PPA) (Zaslavski, A., 2016). In equation (8), $\|Af-g\|_2^2$ can be approximated linearly at current iteration point f^k:

$$\begin{aligned}\|Af-g\|_2^2&\approx\|Af-g\|_2^2+\\&(2M^T(f-f^k))+\frac{1}{\tau}\|f-f^k\|_2^2\end{aligned} \tag{10}$$

Substitute equation (10) into equation (9) and replace $\|Af-g\|_2^2$. And then we use the same method as equation (9) to get the solution.

$$\begin{aligned} f^* = &(\lambda_1 I + \lambda_2 D^T D + \frac{2\rho}{\tau} I)^+ \\ &(\lambda_1 W^T z - W^T \gamma_1 + \lambda_2 D^T v - D^T \gamma_2 - \\ &A^T \gamma_3 - 2\rho A^T (Af^k - g_0) + \frac{2\rho}{\tau} f^k) \end{aligned} \tag{11}$$

The constant matrix $(\lambda_1 I + \lambda_2 D^T D + \frac{2\rho}{\tau} I)$ is easy to diagonalize. formula (11) can be abbreviated as:

$$f^* = F(f, z, v) \tag{12}$$

The second sub-problem about z is L(z):

$$\begin{aligned} z^* = &\arg\min_z(z, v, f) = \alpha_1 \|z\|_0 \\ &+\gamma_1^T (W f - z) + \frac{\lambda_1}{2} \|Wf - z\|_2^2 \end{aligned} \tag{13}$$

Sorting out the above formula (13) and delete the constant terms:

$$z^* = \arg\min_z(z, v, f) = \alpha_1 \|z\|_0 + \frac{\lambda_1}{2} \left\| z - (\frac{\gamma_1^T}{\lambda_1} + Wf) \right\|_2^2 \tag{14}$$

This problem can be solved effectively by the iterative hard-threshold (HST) algorithm (Daubechies, I., 2016) and the expression is:

$$z^* = H_{\sqrt{\frac{2\alpha_1}{\lambda_1}}}(\frac{\gamma_1^T}{\lambda_1} + Wf) = \begin{cases} 0, & \left| \frac{\gamma_1^T}{\lambda_1} + Wf \right| \le \sqrt{\frac{2\alpha_1}{\lambda_1}} \\ \left\{ 0, \frac{\gamma_1^T}{\lambda_1} + Wf \right\}, & \left| \frac{\gamma_1^T}{\lambda_1} + Wf \right| \le \sqrt{\frac{2\alpha_1}{\lambda_1}} \\ \frac{\gamma_1^T}{\lambda_1} + Wf, & \left| \frac{\gamma_1^T}{\lambda_1} + Wf \right| \ge \sqrt{\frac{2\alpha_1}{\lambda_1}} \end{cases} \tag{15}$$

The third sub-problem about ν is L(ν):

$$\begin{aligned} v^* = &\arg\min_v(z, v, f) = \alpha_2 \|v\|_1 \\ &+\gamma_2^T (Df - v) + \frac{\lambda_2}{2} \|Df - v\|_2^2 \end{aligned} \tag{16}$$

Sorting out the above formula and delete the constant terms:

$$v^* = \arg\min_v(z, v, f) = \alpha_2 \|v\|_1 + \frac{\lambda_2}{2} \left\| v - (\frac{\gamma_2^T}{\lambda_2} + Df) \right\|_2^2 \tag{17}$$

This problem can be solved effectively by the iterative soft-threshold (IST) algorithm (Zhang, Y., 2013) and the expression is:

$$v^* = S_{\frac{\alpha_2}{\lambda_2}}(\frac{\gamma_2^T}{\lambda_2} + Df) = \begin{cases} \frac{\gamma_2^T}{\lambda_2} + Df + \frac{\alpha_2}{\lambda_2}, & \frac{\gamma_2^T}{\lambda_2} + Df \le -\frac{\alpha_2}{\lambda_2} \\ 0, & \left\| \frac{\gamma_2^T}{\lambda_2} + Df \right\| \le \frac{\alpha_2}{\lambda_2} \\ \frac{\gamma_2^T}{\lambda_2} + Df - \frac{\alpha_2}{\lambda_2}, & \frac{\gamma_2^T}{\lambda_2} + Df \ge \frac{\alpha_2}{\lambda_2} \end{cases} \tag{18}$$

The pseudo-code of TV-TFIR algorithm is shown in the Table 1.

Table 1: The pseudo-code of the TV-TFIR.

Initializations.
While(n $n \le N_{\max}$) do
Update f : $f^{n+1} = F(f^n, z^n, v^n)$;
Update z : $z^{n+1} = H_{\sqrt{\frac{2\alpha_1}{\lambda_1}}}(\frac{\gamma_1^T}{\lambda_1} + Wf^n)$;
Update v : $v^{n+1} = S_{\frac{\alpha_2}{\lambda_2}}(\frac{\gamma_2^T}{\lambda_2} + Df^n)$;
Lagrange multipliers update: $\gamma_1 \leftarrow \gamma_1 + \lambda_1(W f^{n+1} - z^{n+1})$; $\gamma_2 \leftarrow \gamma_2 + \lambda_2(D f^{n+1} - v^{n+1})$; $\gamma_3 \leftarrow \gamma_3 + \rho(A f^{n+1} - g)$;
If stopping criteria then return f^{n+1}
else n=n+1.

3 EXPERIMENTAL RESULTS

In this paper, the Forbild phantom (Yu, Z., 2012) is used to complete the simulation experiment for different projection numbers. Furthermore, we use the real projection data of a gear to prove the validity of the, algorithm. The Forbild phantom image and the gear image are shown in Fig 2. To show the accuracy of our algorithm, the SART algorithm, the TV algorithm and the TFIR algorithm are used to contrast experiments.

First, a simulated Forbild phantom is used to certify the performance of TV-TFIR algorithm on

spatial resolution and accuracy. And real projection data of Gear is used to certify the performance of TV-TFIR algorithm.

In order to quantify the experimental results, the quantitative index root mean square (RMSE), peak signal-to-noise ratio (PSNR) and structural similarity (SSIM) and the quantitative index are utilized as follows (Zhou Wang, A.C., 2004):

$$\mathrm{RMSE} = \sqrt{\frac{\sum_{i,j} (\mathrm{f}_{i,j} - \mathrm{f}^{*}_{i,j})^2}{N_{pixel}}} \tag{19}$$

$$PSNR = 10 \log_{10} \frac{(\max(\mathrm{f}_{i,j}))^2}{\sum_{i,j} (\mathrm{f}_{i,j} - \mathrm{f}^{*}_{i,j})^2 \Big/ N_{pixel}} \tag{20}$$

$$SSIM(\mathrm{X}, \mathrm{Y}) = \frac{(2u_x u_y + \mathrm{C}_1)(2\sigma_{XY})}{(u_X^2 + u_Y^2 + \mathrm{C}_1)(\sigma_X^2 + \sigma_Y^2 + \mathrm{C}_2)} \tag{21}$$

Where f is the reconstructed image and $f_{i,j}$ ang $f^{*}_{i,j}$ respectively are the pixel value of the image f and the reference image. N_{pixel} is the pixel number of the image f .

All experiments are implemented on a personal computer (PC) with an Inter(R) Xeon(R) CPU E3-1231 v3 @3.4GHz and 16GB RAM. The programming language used in the experiment is MATLAB and C++.

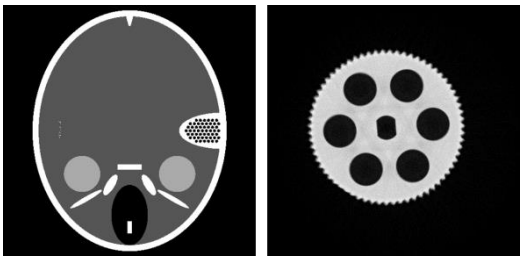

Figure 2: The Images used in the experiment. a) The Forbild phantom; b) The Gear image.

3.1 Results on Forbild Phantom

In the simulation experiment, a simulated Forbild phantom with 512*512 pixels is used to prove the validity of our algorithm, and the image is shown in Fig 2 a). The lower part of the simulated forbild phantom includes some ellipses and rectangles with different gray values. On the right side of the phantom, there is a half ellipse with high gray value, and there are many small circles with low gray value inside the ellipse. The left side of the module has some randomly distributed high gray value points. The gray value is uniform in other parts of the model except for a circle with higher gray value.

This Forbild phantom is consistent with medical and industrial applications. The parameters of the simulated image scanning system are shown in the table 2.

Table 2: Geometry scanning parameters of exterior CT for the simulated imaging system

Simulated system parameter	Parameter
Distance X-ray to center	900.0 mm
Distance center to detector	500.0 mm
The number of detector units	372
The length of the detector	372 mm
Image size	512 × 512
The pixel size of the image	1.0 × 1.0

For the simulation experiment, the SART algorithm, TV algorithm and TFIR algorithm are used as the contrast experiments. The projection angles used in the experiment are respectively 30 views, 40 views and 50 views. The results of the Forbild phantom are shown in Fig 3. The phantom reconstructed using SART has severe linear artifacts. The linear artifacts in the results of TV are much less when the projection angles are enough. The results of TFIR are no linear artifacts. But the result of the TFIR method will lead to deformation of image details as shown in Fig 4. Compared with the SART, TV and TFIR, the results of the proposed algorithm are recovered more accurately.

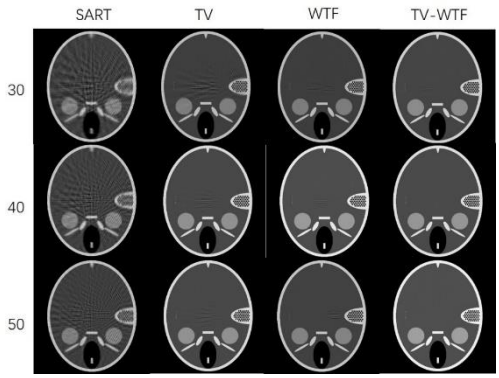

Figure 3: The simulated experiment results of the Forbild phantom.

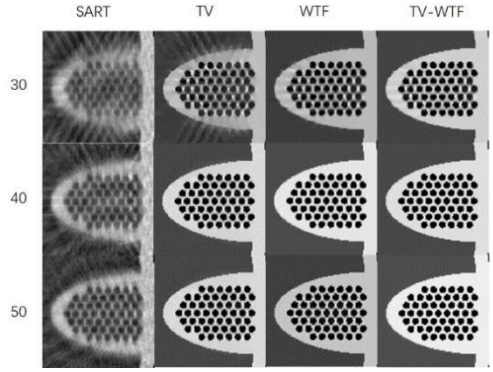

Figure 4: The reconstructed ROIs of the Forbild phantom in Figure 3.

Figure 5 shows the quantitative indicators of the reconstruction results of the Forbild phantom images. And in the paper, RMSE, PSNR and SSIM are respectively used as quantitative indicators. Each sub-figure in figure 5 contains three sets of histograms. They represent the quantitative indicators at projection views of 30, 40 and 50 respectively. And each group of histograms consists of four histograms, which respectively represent the four algorithms used in the experiment. As can be seen from figure 5, the result of quantitative index is consistent with the visual effect in figure 3. The SART algorithm performs worst, and the quantitative indicators and visual effects of TV and TFIR are little difference. Our proposed algorithm performs best.

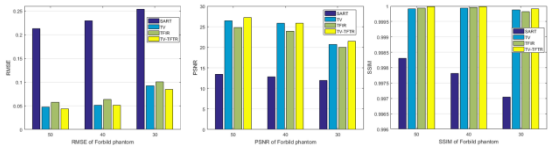

Figure 5: a) RMSE, b) PSNR and c) SSIM of the Forbild phantom results.

The convergence analysis is shown in Fig 6 that shows the RMSE values with the iterations number. Fig 6 shows that the error decreases fastest at the beginning of the iteration and stops falling as iterate 1000 steps. The plot shows the proposed algorithm can minimize the RMSE. And combined with Fig 5, it can be found that our method can always achieve RMSE minimization in different projection views.

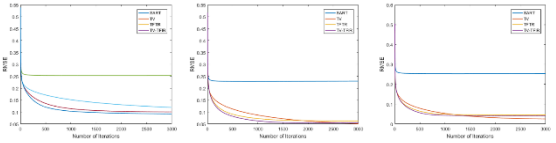

Fig 6: RMSE as a function of the number of iterations for the Forbild phantom study. (a) 30 views, (b) 40 views, (c) 50 views.

3.2 Result on Real Data

To evaluate the effectiveness of TV-TFIR algorithm in practical applications field, real projection data of a Gear is used to verify the TV-TFIR algorithm. The pixels of the gear image are 512*512. The scanning parameters are shown in table 3.

Table 3: Geometry scanning parameters of exterior CT for the real imaging system

System parameter	Parameter
Distance X-ray to center	1950.0 mm
Distance X-ray to detector	148.86 mm
The number of detector units	553
The length of the detector	42 mm
Image size	512 × 512
Pixel size	0.076 × 0.076

For the real data experiment, the SART algorithm, TV algorithm and TFIR algorithms are used as the contrast test. The projection views used in the experiment are respectively 37 views and 48 views.

Figure 7 shows the reconstruction results of the Gear image. Figure 8 shows the ROIs of the Gear image. As shown in Figure 7 and Figure 8, SART results are the worst, with noise and artifacts distributed throughout the image. The result of the TV algorithm is smooth, and the brightness and smoothness are similar to the Gear image in Figure 2 (b). But the TV results are fuzzy on the edges. The result of TFIR is good for edge reconstruction, but there are artifacts in the whole image, and the gray level is obviously inconsistent with the Figure 2 (a). The TV-TFIR algorithm is similar to TV in terms of the smoothness of the image. But the TV-TFIR algorithm is superior to TV algorithm for image edge reconstruction. However, the algorithm we proposed is inferior to TFIR algorithm in edge preserving. In general, our algorithm is superior to other algorithms.

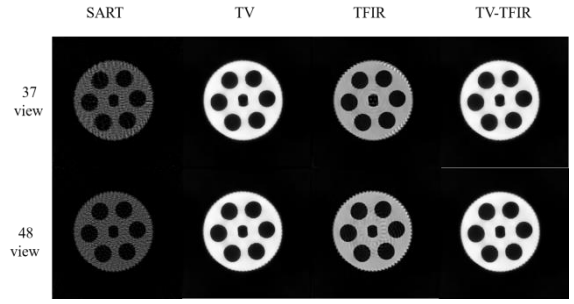

Figure 7: The real data experiment results of the Gear.

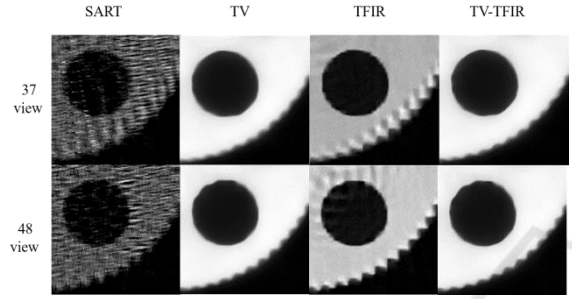

Figure 8: The reconstructed ROIs image in Fig 7.

4 DISCUSSION & CONCLUSION

Short-scanning few-view computer tomography (SSFV-CT) is an effective method to reduce the radiation dose. TV algorithm and tight frame iteration regularization algorithm are widely used in CT reconstruction for incomplete projection data. But TV algorithm assumes the image is piecewise constant and that doesn't satisfy the clinical and industrial reality. Furthermore, it may lead to blocky artifacts in reconstructed image. Tight frame regularization algorithm can prevent the appearance of blocky artifacts, but it can't reconstruct high quality images when the projection data is seriously incomplete. In the paper, we proposed an image reconstruction total based on variation and tight frame iteration regularization for short-scanning few-view computer tomography.

There are several parameters to choose in the experiment, we use trial and error method to select the parameters in this paper. Although the parameters used may not be optimal, the experimental results show that the proposed method can reconstruct the image with higher quality.

One disadvantage of our proposed algorithm is computationally intensive. But with the development of high-performance computing devices, computing power may not be the biggest bottleneck in the future.

In conclusion, the proposed algorithm can adapt the severely incomplete projection data.

ACKNOWLEDGEMENTS

The work is supported by Ministry of The "ChunHui Plan" Fund Project of the Ministry of Education (Z2014 085) and Chongqing Municipal Education Commission Project (KJ1601210) in College of Big Data and Intelligent Engineering, Yangtze Normal University.

REFERENCES

Abushammala, M., Khuri, S. A., & Sayfy, A. (2015). A novel fixed point iteration method for the solution of third order boundary value problems. Applied Mathematics & Computation, 271(C), 131-141.

Andersen, A. H., & Kak, A. C. (1984). Simultaneous algebraic reconstruction technique (sart): a superior implementation of the art algorithm. Ultrasonic Imaging, 6(1), 81-94.

Brenner, D. J. , & Hall, E. J. . (2007). Computed tomography-an increasing source of radiation exposure. New England Journal of Medicine, 357(22), 2277-2284.

Chang, S. S. Peterson, R. J. & Ho, C. T. (1978). Chemical reactions involved in the deep-frying of foods. Journal of the American Oil Chemists' Society, 55(10), 718-727.

Daubechies, I., Defrise, M., & Mol, C. D. (2016). Sparsity-enforcing regularisation and ista revisited. Inverse Problems, 32(10), 104001.

Donoho, D. L. (2006). Compressed sensing. IEEE Transactions on Information Theory, 52(4), 1289-1306.

Gu, J., & Ye, J. C. (2017). Multi-scale wavelet domain residual learning for limited-angle ct reconstruction.

Hsieh, J., Molthen, R. C., Dawson, C. A., & Johnson, R. H. (2000). An iterative approach to the beam hardening correction in cone beam ct. Medical Physics, 27(1), 23-29.

Jouini, M. S., & Keskes, N. (2016). Numerical estimation of rock properties and textural facies classification of core samples using x-ray computed tomography images. Applied Mathematical Modelling, 41.

Laroque, S. J., Sidky, E. Y., & Pan, X. (2008). Accurate image reconstruction from few-view and limited-angle data in diffraction tomography. Journal of the Optical Society of America A Optics Image Science & Vision, 25(7), 1772-82.

Li, J. , Zhang, W. , Cai, A. , Wang, L. , Liang, N. , & Zheng, Z. , et al. (2018). Joint regularization-based image reconstruction by combining data-driven tight

frame and total variation for low-dose computed tomography. Journal of X-ray science and technology.

Li, M., Fan, Z., Ji, H., & Shen, Z. (2014). Wavelet frame based algorithm for 3d reconstruction in electron microscopy. Siam Journal on Scientific Computing, 36(1), B45-B69.

Lu, Y. , Zhao, J. , & Wang, G. . (2011). Few-view image reconstruction with dual dictionaries. Physics in Medicine & Biology, 57(1), 173-189.

Peng, J., Roos, C., & Terlaky, T. (2000). New complexity analysis of the primal—dual newton method for linear optimization. Annals of Operations Research, 99(1-4), 23-39.

Ritschl, L., Bergner, F., Fleischmann, C., & Kachelriess, M. (2011). Improved total variation-based ct image reconstruction applied to clinical data. Physics in Medicine & Biology, 56(6), 1545-61.

Sidky, E. Y. , & Pan, X. . (2008). Image reconstruction in circular cone-beam computed tomography by constrained, total-variation minimization. Physics in Medicine & Biology, 53(17), 4777-4807.

Unser, M., Aldroubi, A., & Eden, M. (1992). On the asymptotic convergence of b-spline wavelets to gabor functions. IEEE Trans.inform.theory, 38(2), 864-872.

Wang, G. , Yu, H. , & Ye, Y. . (2009). A scheme for multisource interior tomography. Medical Physics, 36(8), 3575-3581.

Wang, Y., Yang, J., Yin, W., & Zhang, Y. (2016). A New Alternating Minimization Algorithm for Total Variation Image Reconstruction. International Conference on Wireless, Mobile and Multi-Media (Vol.1, pp.248-272). IET.

Xu, Q. , Yu, H. , Mou, X. , Zhang, L. , Hsieh, J. , & Wang, G. . (2012). Low-dose x-ray ct reconstruction via dictionary learning. IEEE Transactions on Medical Imaging, 31(9), 1682-1697.

Yu, H. , & Wang, G. . (2009). Compressed sensing based interior tomography. Physics in Medicine & Biology, 54(9), 2791-805.

Yu, W. , & Zeng, L. . (2015). ℓ0 gradient minimization based image reconstruction for limited-angle computed tomography. Plos One, 10(7), e0130793.

Yu, W. , Wang, C. , Nie, X. , Huang, M. , & Wu, L. . (2017). Image reconstruction for few-view computed tomography based on ℓ 0, sparse regularization ☆. Procedia Computer Science, 107, 808-813.

Yu, Z. , Noo, Frédéric, Dennerlein, F. , Wunderlich, A. , Lauritsch, Günter, & Hornegger, J. . (2012). Simulation tools for two-dimensional experiments in x-ray computed tomography using the forbild head phantom. Physics in Medicine and Biology, 57(13), N237-N252.

Zaslavski, A. J. (2016). Proximal Point Algorithm. Approximate Solutions of Common Fixed-Point Problems. Springer International Publishing.

Zhang, L. , Zeng, L. , & Guo, Y. . (2018). L0 regularization based on a prior image incorporated non-local means for limited-angle x-ray ct reconstruction. Journal of X-Ray Science and Technology, 26(8), 1-18.

Zhang, Y. , Dong, B. , & Lu, Z. . (2013). L0 minimization for wavelet frame based image restoration. Mathematics of Computation, 82(282), 995-1015.

Zhou Wang, A.C. Bovik, H.R. Sheikh, & E.P. Simoncelli. (2004). Image quality assessment: from error visibility to structural similarity. IEEE Trans Image Process, 13(4), 600-612.